A Method for Studying Conformational Relaxations by Molecular Simulation: Conformational Defects in α-Phase Poly(vinylidene fluoride)

Jeffrey D. Carbeck[†] and Gregory C. Rutledge*[,‡]

Department of Chemical Engineering, Massachusetts Institute of Technology, Cambridge, Massachusetts 02139

Received February 1, 1996; Revised Manuscript Received April 19, 1996[⊗]

ABSTRACT: A general method is proposed for the molecular level characterization of relaxation and transformation processes in polymer crystals mediated by propagation of conformational imperfections. The proposed approach combines a definition of the defect ensemble, in terms of the extent and boundary conditions of the defect zone, with procedures for searching conformation space for stable conformations in the ensemble and for determining the adiabatic reaction path connecting one symmetry-equivalent position of the defect in the lattice to another. The method was applied to the α_c relaxation that occurs in the crystalline α phase of PVDF (α-PVDF). A large number of possible defects were found with a wide spectrum of heats of formation. Several of the lowest energy defects could be packed efficiently into the α-PVDF crystal. The adiabatic pathway for defect transport was estimated and vibrational contributions to the thermodynamic functions were obtained at all the stationary states. Two distinct relaxation processes were found. One exhibits a large intermolecular packing energy contribution to its heat of formation and must traverse free-energy barriers of 6−9 kcal/mol to propagate through the crystal, while the other exhibits a large intramolecular conformational energy contribution to its heat of formation but may propagate with free-energy barriers of about 2.4 kcal/mol. The intermediate states for this latter process involve short all-trans segments, suggesting that this may also be a mechanism for the α-to-γ and α-to-β phase transitions.

1. Introduction

Conformational relaxations mediate the physical properties of solid polymers through translation and rotation of chain segments and transport of small impurities or voids. Relaxation spectra measured by mechanical, dielectric, or NMR spectroscopy give identifiable peaks which are often attributed to discrete mechanisms such as side-chain or backbone motion. Understanding the behavior of different polymeric materials requires relating these mechanisms to the underlying chemistry. Molecular simulations provide a powerful tool for identifying and testing these molecular level descriptions directly by allowing for and tracking the behavior of dynamic processes which are consistent with the observed structural relaxation. Molecular dynamics (MD) represents a potentially useful method for such studies at very short time scales. However, many dynamic processes in polymers do not lend themselves to study within the tens of nanoseconds currently accessible by MD simulations. In particular, processes which occur with frequencies in the gigahertz range or lower are poorly sampled in such simulations. Notable examples include the crystalline α relaxations (α_c) in many semicrystalline polymers, crystal annealing processes, and solid−solid transitions which occur upon application of stress or electric fields. By no means exhaustive, these examples, associated with the ordered crystalline region, lend themselves in many cases to particularly simple models.

The α_c relaxation in polyethylene has been addressed by numerous models which account for rotation of a chain in the crystal lattice, in accord with dielectric relaxation measurements.[1] Conformational defects have long been proposed as a mechanism for the α_c relaxation in alkane polymers. Reneker and co-workers, using potential energy minimizations, have cataloged a variety of conformational defects in polyethylene (PE) crystals.[2−4] Mansfield and Boyd demonstrated that a localized twist in an all-trans chain of polyethylene could propagate with little barrier and that the energetics of the twist, in combination with a gradually attenuated displacement of the repeat units, could explain the dependence of the relaxation frequency on lamellar thickness.[5] This mechanism was generalized when it was realized that the equations of motion of the twist had soliton-like solutions.[6] Skinner and Wolynes developed a model of Brownian diffusion of solitons in PE,[7,8] and Skinner and Park[9] later showed that this model could predict the temperature-dependent dielectric relaxation curves of PE over a wide range of frequencies.

A similar process is the α_c relaxation in the α phase of isotactic polypropylene (iPP). Two-dimensional solid-state NMR studies on iPP suggested a helical jump mechanism whereby the 3_1 helix of iPP rotated 120° with a frequency on the order of 1 s.[10] As in PE, it was proposed that the α_c relaxation in iPP results from independent processes occurring in single chains. In an extension of the work on PE, Syi and Mansfield applied the soliton model to a number of helical polymers, including iPP, which can support a solitary wave.[11] They assumed that the soliton moves along a potential energy surface characterized by screw displacement of a single repeat unit in the lattice. Rutledge and Suter[12] used molecular mechanics calculations to estimate the activation energy for concerted rotations of the polymer helix, where each repeat of the chain undergoes the same screw displacement simultaneously, and the energy of formation of interstitial- or vacancy-type dispiration defects, which effect a screw displacement of the chain via a hopping mechanism.

In contrast with the α_c relaxation in PE and iPP, the α_c relaxation in the α phase of poly(vinylidene fluoride)

* To whom correspondence should be addressed.
[†] Department of Materials and Science and Engineering.
[‡] Department of Chemical Engineering.
[⊗] Abstract published in *Advance ACS Abstracts,* June 1, 1996.

S0024-9297(96)00165-9 CCC: $12.00

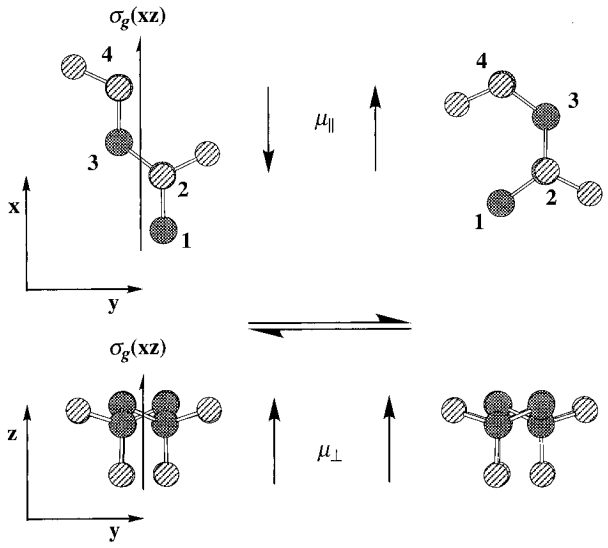

Figure 1. Change in the repeat unit conformation due to the α_c relaxation in α-PVDF.

(α-PVDF) entails a change in conformation of the chain, as shown in Figure 1. The dielectric relaxation studies of Miyamoto *et al.*[13] demonstrated that the α_c relaxation in α-PVDF involves reversal of the dipole moment parallel to the chain axis only and proposed that this reversal occurs through the conformational change $TGT\bar{G} \leftrightarrow \bar{G}TGT$, consistent with later X-ray studies.[14] Two-dimensional solid-state NMR confirmed this relaxation mechanism and found that the relaxation also involves a change in orientation of the C−H bond by 113°.[15] The NMR results also indicated that the relaxation involves the switching of the chain between two sites and that all the segments in a chain reorient.

Due to this change in conformation, the α_c relaxation in α-PVDF does not lend itself to description by gradual twists in or concerted rotation of helices in the crystalline lattice. As is generally the case, there is no obvious *a priori* candidate defect conformation for the α_c relaxation in α-PVDF. Instead, techniques must be developed to search conformation space for candidate defects that satisfy a set of boundary conditions suggested by experiment. Once candidate defects are identified, their energies and mobilities may be examined to determine their likelihood as mechanisms for the relaxation.

In an initial study, Clark *et al.* calculated the energy to create a defect in a single chain of α-PVDF that could accomplish the conformational rearrangement of the α_c relaxation.[16] They found defects that had a barrier to propagation in a single chain of approximately 9 kcal/mol. In comparing these calculated barriers to the activation free energy of ≪1 kcal/mol obtained by Miyamoto *et al.*,[13] Clark *et al.* concluded that these defects were excluded as candidates for the α_c relaxation. However, the estimates of activation energy by Miyamoto *et al.* appear to be on a *per repeat unit* basis and cannot be directly compared to the energy of defect formation and propagation. Also, it is not clear that a comprehensive search of defect conformation space was obtained, and there was no investigation of the interaction of the defect with the surrounding lattice.

In this work, we develop a general procedure to approach this type of problem using molecular simulations. This procedure involves two stages. In the first stage, the analytical techniques of Gō and Scheraga[17] are used to identify conformations of a segment of chain which can splice together the two chain segments which confine a defect. The energetics of defect formation are studied using an empirical potential energy expression and a normal-mode analysis to calculate the vibrational free energy. In the second stage the mobility of these defects is estimated by calculating the adiabatic reaction pathway for defect transport along the chain. We focus the application of this procedure to the study of the α_c relaxation in α-PVDF.

2. Computational Method

The basic idea behind any defect-mediated relaxation or transition entails two components: the formation of a defect within the perfect lattice and the propagation of this defect through the lattice. Defects that have a favorable free energy of formation but have energy barriers too large for propagation do not lead to observable relaxations. The method proposed here involves two stages. First, a search procedure is described for identifying low-energy conformations which bridge the "before" and "after" states of the single chain undergoing relaxation. The probabilities of these "bridge" or defect states are characterized in terms of their energies of formation. Second, a saddle-point search technique is employed to identify low-energy paths across the energy surface which translate the defect by one lattice period along the chain. Periodicity of the crystal lattice in this case ensures that these conditions are sufficient to fully describe propagation of the defect through the lattice in the chain direction. In this treatment, we do not consider the possibility of translation lateral to the chain direction.

2.1. Boundary Conditions. In order for the method to be generally applicable, "before" and "after" states of the single chain must be known. This is generally possible from wide-angle X-ray diffraction measurements or spectroscopic methods such as those mentioned previously. Other considerations such as the number of chemical repeat units participating in the defect and the nature of the defect line complete the specification of boundary conditions for candidate defect structures. Defect lines for lattice defects are well-known in small molecule crystallography,[18] and their description in polymeric solids has been summarized by Reneker and Mazur.[4] The most important cases for lattice defects involving single chains within the crystal lattice are dislocations, involving translational offsets of repeat units along the chain, disclinations, involving rotation of one part of the chain with respect to the other, and dispirations, which may be thought of as defects of helical symmetry and involve the combination of a partial dislocation and a partial disclination. Dislocations and dispirations may be further categorized as either interstitial or vacancy types, depending upon the sign of the translational offset. Disclinations need not involve interstitial atoms or vacancies. Defects connecting "before" and "after" states of different conformation, such as that required for the α_c relaxation in α-PVDF, cannot be described by such defect lines but instead are bounded by distinctly different but regular conformations.

The issue of defect extent, the number of repeat units over which the bridging transition occurs, is less well-defined. In principle, the extent of the defect is limited only by the length of the chain, for a conformational defect, or the extent of the crystal lattice itself. From a practical point of view, however, it is reasonable to consider localized defects as a first approximation, as

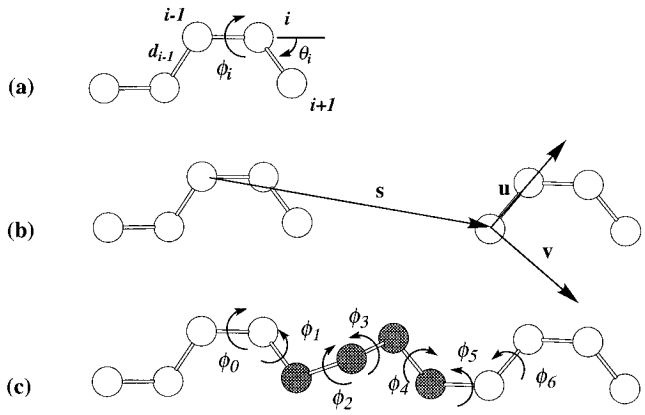

Figure 2. (a) Definition of chain geometry; d_i, bond length; θ_i, bond angle, ϕ_i, backbone torsion. (b) Vectors **s**, **u**, and **v**, that define the transformation between the two segments. (c) Conformational search for defect structures. ϕ_0 is scanned 360° in 15° increments, and ϕ_1 through ϕ_6 are determined analytically.

these involve the least distortion of the crystal lattice. This is the approach followed in this work. Consideration of the spreading tendency of a localized defect and generalization to defects of a greater extent may be dealt with subsequently.

2.2. Construction of the Defect Ensemble. The defect ensemble, by analogy to the canonical ensemble of statistical mechanics, consists of the individual states which satisfy the constraints of particle number (the extent of the defect), volume (or length, in the current case of single-chain conformational defects), temperature, and boundary conditions, as described above. Our goal in the first stage of the procedure is to identify a practical method for sampling the most important states in the ensemble.

For studies of conformational defects confined to a single chain, the method developed by Gō and Scheraga for calculating conformational rearrangements in linear polymers, under the conditions of fixed bond lengths and bond angles, represents a powerful tool.[17] The method has since been used as the basis for a Monte Carlo step in the simulation of bulk amorphous polymers[19] and has been generalized to systems of variable bond length and bond angle.[20] As originally proposed, fixing the position of two chain segments in space allows the definition of two unique local coordinate systems: one at the end of the first segment (the "before" state) and one at the beginning of the second (the "after" state). A local orthogonal coordinate system is defined for any atom, i, by defining the origin as the position of atom $i - 1$, the x-axis as lying along the bond from $i - 1$ to i, and the y-axis such that atom $i + 1$ lies in the positive quadrant of the xy plane; the z-axis is fixed by orthogonality. The transformation of a coordinate r_i in the local frame of atom i to r_{i-1} in the local frame of atom $i - 1$ is expressed as

$$r_{i-1} = \mathbf{T}_{i-1}\mathbf{R}_i r_i + \mathbf{p}_i \tag{1}$$

where $\mathbf{p}_i$, $\mathbf{T}_i$, and $\mathbf{R}_i$ are defined in terms of bond length, d_i, bond angle, θ_i, and bond torsion, ϕ_i (see Figure 2a), as follows (the superscript T denotes the vector transpose):

$$\mathbf{p}_i = (d_i, 0, 0)^{\mathrm{T}} \tag{2}$$

$$\mathbf{T}_i = \begin{pmatrix} \cos\theta_i & -\sin\theta_i & 0 \\ \sin\theta_i & \cos\theta_i & 0 \\ 0 & 0 & 1 \end{pmatrix} \tag{3}$$

$$\mathbf{R}_i = \begin{pmatrix} 1 & 0 & 0 \\ 0 & \cos\phi_i & -\sin\phi_i \\ 0 & \sin\phi_i & \cos\phi_i \end{pmatrix} \tag{4}$$

The location and orientation of the second segment with respect to the first segment can be expressed by three vectors: **s**, the position of the first atom of the second segment; **u**, a unit vector along the first bond of the second segment (the x-axis of the local coordinate system of the second segment); and **v**, a unit vector parallel to the y-axis of this same local coordinate system (as shown in Figure 2b). Under the conditions of fixed bond lengths and bond angles, six equations in six unknowns may then be specified by repetitive application of eq 1:

$$\mathbf{s} = \mathbf{p}_0 + \mathbf{T}_0\mathbf{R}_1\mathbf{p}_1 + \mathbf{T}_0\mathbf{R}_1\mathbf{T}_1\mathbf{R}_2\mathbf{p}_2 + \ldots + \mathbf{T}_0\mathbf{R}_1\mathbf{T}_1\mathbf{R}_2\ldots\mathbf{T}_4\mathbf{R}_5\mathbf{p}_5$$

$$\mathbf{u} = \mathbf{T}_0\mathbf{R}_1\mathbf{T}_1\mathbf{R}_2\ldots\mathbf{T}_4\mathbf{R}_5\mathbf{T}_5\mathbf{R}_6\mathbf{e}_1 \tag{5}$$

$$\mathbf{v} = \mathbf{T}_0\mathbf{R}_1\mathbf{T}_1\mathbf{R}_2\ldots\mathbf{T}_4\mathbf{R}_5\mathbf{T}_5\mathbf{R}_6\mathbf{e}_2$$

subject to the constraints $\mathbf{u}\cdot\mathbf{u} = 1$, $\mathbf{v}\cdot\mathbf{v} = 1$ and $\mathbf{u}\cdot\mathbf{v} = 0$. $\mathbf{e}_1$ and $\mathbf{e}_2$ are the unit vectors $(1, 0, 0)^{\mathrm{T}}$ and $(0, 1, 0)^{\mathrm{T}}$, respectively.

For a given position of the two fixed segments there may be 0, 2, 4, 6, ... sets of torsion angle solutions, which fully enumerate the allowable local conformations under the constraints of fixed bond lengths and bond angles. Calculation of the sets of torsion angle solutions requires the finding of roots of a nonlinear equation, a problem solved numerically using Brent's method.[21] The determination of six consecutive torsions allows three atoms to participate in the local conformation. To extend this to four carbon atoms necessary to span one conformational repeat along the chain in α-PVDF, we scanned one additional torsion angle through 360° in 15° increments and solved for the remaining six torsions, as shown in Figure 2c.

For the case of fixed bond lengths and bond angles, the bridging defects identified for the single chain may simply be inserted into the environment of the perfect crystal lattice and the total potential energy computed using an appropriate empirical force field. In crystalline systems this generally leads to a vast reduction in the number of statistically important defect conformations, due to high intermolecular energies. It is of greater practical value to relax the constraints of fixed bond lengths and bond angles and determine the conformations corresponding to the local energy minimum in the expanded phase space of variable bond lengths and angles. This results in structures of lower potential energy as well as allows for calculation of free energies in the harmonic approximation. It may be noted that this procedure does not guarantee the identification of all local minima in Cartesian coordinates, due to the initial step with constrained internal coordinates. However, under the conventional assumption that variations in the soft, torsion angles are most critical, we expect this procedure to identify rapidly the majority of important defect conformations. Such separation and stepwise inclusion of "soft" and "hard" degrees of

freedom has a long and productive history in polymer modeling.[22−24] The resulting collection of defect conformations is a set of stable, energetically-representative conformers which satisfy the constraints of extent and such boundary conditions as are consistent with the observed relaxation.

In the case of α-PVDF, we relaxed the constraints of fixed bond lengths and angles required by the method of Gō and Scheraga by performing energy minimizations with respect to the four backbone carbon atoms and eight substituent hydrogen and fluorine atoms involved in the defect. The coordinates of the substituent hydrogen and fluorine atoms on the two carbon atoms adjacent to the four-atom defect were also included in the minimization. (The coordinates of the two carbon atoms adjacent to the four-atom defect were not included in this minimization.) The energy of selected, low-energy candidate defects was further minimized in a crystal environment. A six repeat unit chain containing the defect was surrounded by a rigid shell of nearest-neighbor chains without defect at the experimental lattice spacings: $a = 4.96$ Å, $b = 9.64$ Å, $c = 4.62$ Å (see Figure 3). In this case, only the first and last repeat units of the chain containing the defect were held fixed.

2.3. Determination of the Relaxation Pathway. In order to characterize the mobility of a particular conformational defect along the chain direction in the crystalline environment, one requires at least the lowest energy transition state for the translation of the defect along the chain by one period of the lattice. Ideally, the entire reaction coordinate can be determined, including multiple intermediary transition states comprising a complex reaction coordinate. In their work on solitonic motion in crystalline polymers, Syi and Mansfield assumed the coordinate for propagation of the solitary wave occurred on the potential energy surface determined by a concerted screw displacement of one chain in the crystal lattice from one equivalent position to the next.[11] In our approach, we employ the conjugate peak refinement technique of Fischer and Karplus[25] to identify the adiabatic reaction paths connecting two equivalent positions for the defect in the lattice. In this technique the pathway between two minima is determined iteratively through a series of steps that consist of (1) determining the maximum along the linear interpolation vector $s = x_i - x_j$ connecting two states, i and j (x_i and x_j are the coordinate vectors for states i and j), on the trajectory, followed by (2) minimization of the energy in the conformation subspace conjugate to s to identify a third point along the trajectory intermediate between i and j. Depending upon the results of the maximization and minimization, a single intermediate point is either added, refined, or removed until the only local maxima in energy left along the path are true saddle points. The method requires only function evaluations and first derivatives of the potential energy function.

One advantage of this technique is that it readily adapts itself to the complexity of the energy surface and can identify multiple transition states along a lowest energy reaction coordinate between two minima. Unlike other algorithms (e.g., that of Cerjan and Miller[26]) it does not rely on a good initial guess of the transition state itself or foreknowledge of the number of such states that might be involved. Intermediary minima and saddle points may be refined using standard minimization algorithms: at a local minimum, the potential energy itself is minimal; at a saddle point, the squared modulus of the gradient of potential energy is minimal. The reaction pathway so-determined is a close approximation to the adiabatic reaction path between equivalent positions for the defect in the lattice.

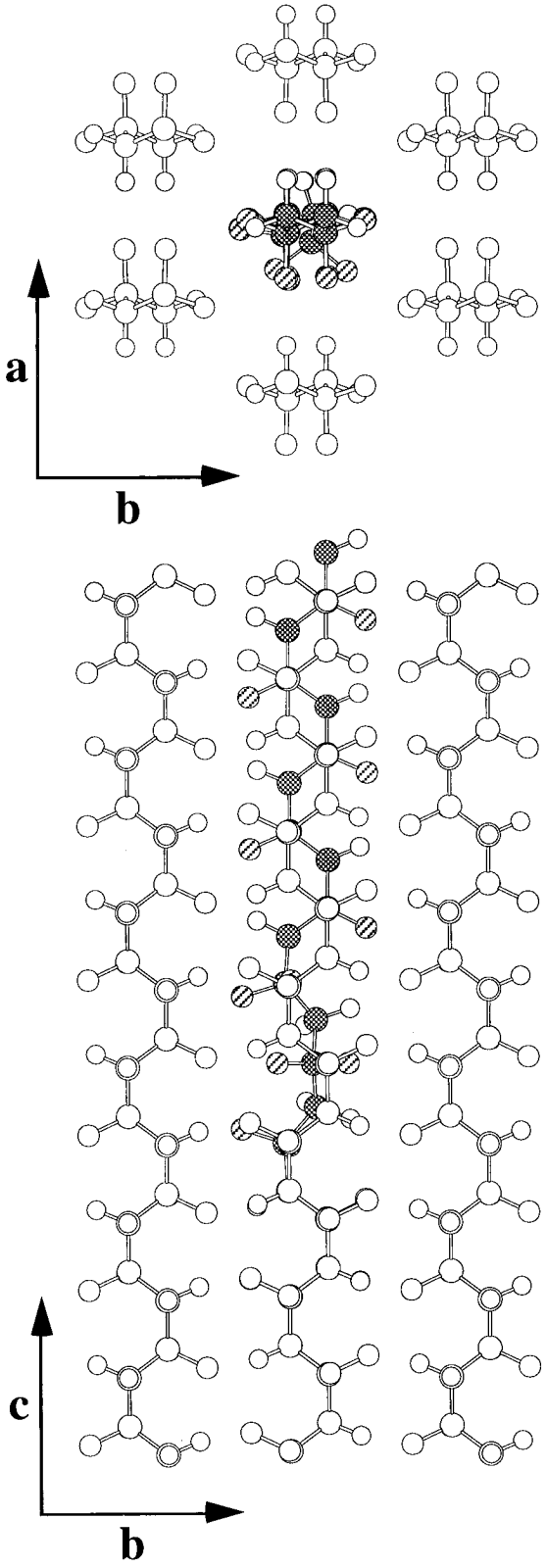

Figure 3. Divergent defect surrounded by a shell of six nearest-neighbor chains.

Vibrational contributions to the free energy are computed for all stationary points along the reaction pathway. Diagonalization of the matrix of analytical second derivatives of the force field with respect to Cartesian displacement of atoms yields the set of $3N$

$(3N - 1)$ normal-mode frequencies for each local minimum (saddle point). From the normal-mode frequencies the vibrational thermodynamic functions are calculated in the harmonic approximation using the standard equations of statistical mechanics.[27] The resulting Helmholtz free energy for stationary points along the adiabatic reaction pathway is then determined as the sum of the potential energy and the vibrational free energy at each point. The loss of 1 degree of freedom at a transition state generally contributes to a significant loss in vibrational entropy relative to a local minimum and hence an increase in activation energy barriers to defect transport, all else being equal.

3. Application to α-PVDF

3.1. Force Field. For PVDF we used a modified version of the MSXX force field developed by Karasawa and Goddard.[28] This force field was parametrized by fitting to *ab initio* calculations of 2,2-difluoropropane and to the experimental vibrational spectra of PVDF in the β phase. The torsional potentials were parametrized to the *ab initio* torsional potential curve of the central C−C bond of 1,1,1,3,3-pentafluorobutane. The MSXX force field yields reasonable energies and vibrational spectra not only for the β phase but also for the α phase and several other known PVDF crystal structures.[28] The modified version of the force field, which we denote MSXX*, differs in its van der Waals parameters for fluorine as described in further detail in refs 29 and 30, where it was employed successfully in the simulation of the temperature-dependent properties of β-PVDF.

3.2. Boundary Conditions for α-PVDF. A combination of dielectric relaxation, X-ray, and NMR studies indicate that the α_c relaxation in α-PVDF involves a reversal of the dipole moment along the chain, $\mu_{||}$, and a change in conformation of TGT$\bar{\text{G}}$ ↔ $\bar{\text{G}}$TGT (see Figure 1). This observation may be compatible with either of two sets of boundary conditions, distinguished by the relative orientation of $\mu_{||}$ on either side of the defect, as shown in Figure 4. In the first, which we refer to as the "divergent" boundary condition, $\mu_{||}$ on either side of the defect points away from the defect and toward the ends of the chain. In the second, which we refer to as the "convergent" boundary condition, $\mu_{||}$ on either side of the defect points toward the defect and away from the ends of the chain. In addition, for both the convergent and divergent boundary conditions, there are four unique initiating points for the defect corresponding to the four unique atoms of the conformational repeat unit (see Figure 1), resulting in a total of eight unique boundary conditions.

Because the conformations of the chain segments on either side of the defect are different, one must also determine the appropriate *c*-axis translation of the transformed segment of the chain—that is, the segment of the chain through which the defect has already passed. To discuss the *c*-axis translation, we refer to the position along *c* of the fluorine-bearing carbon atoms in the transformed segment relative to their original position in the untransformed segment. Figure 1 demonstrates the condition of zero *c*-axis translation; carbons 2 and 4 maintain identical positions along the *c*-axis. (In fact, they maintain identical positions along *a* and *b* as well.) Other energetically favorable positions for the transformed segment involve either a $+c/4$ translation or a $-c/4$ translation of the segment, resulting in vacancy- and interstitial-type defects, respectively. With the four-carbon defects considered in this study, vacancy-type defects were precluded by the initial constraint of fixed bond length and bond angles; interstitial-type defects were precluded by excessive intermolecular packing energies due to the resultant "bulges" which could not pack efficiently into the lattice. Thus, in all our calculations reported here, the transformed segment has zero *c*-axis translation. Further refinement of this registry condition was deemed unjustified in light of the approximations already invoked in assuming the regular perfect lattice; X-ray studies indicate that neighboring chains in the real α-PVDF crystal are distributed statistically among orientations differing by 180° about the *b* and *c* axes.[14]

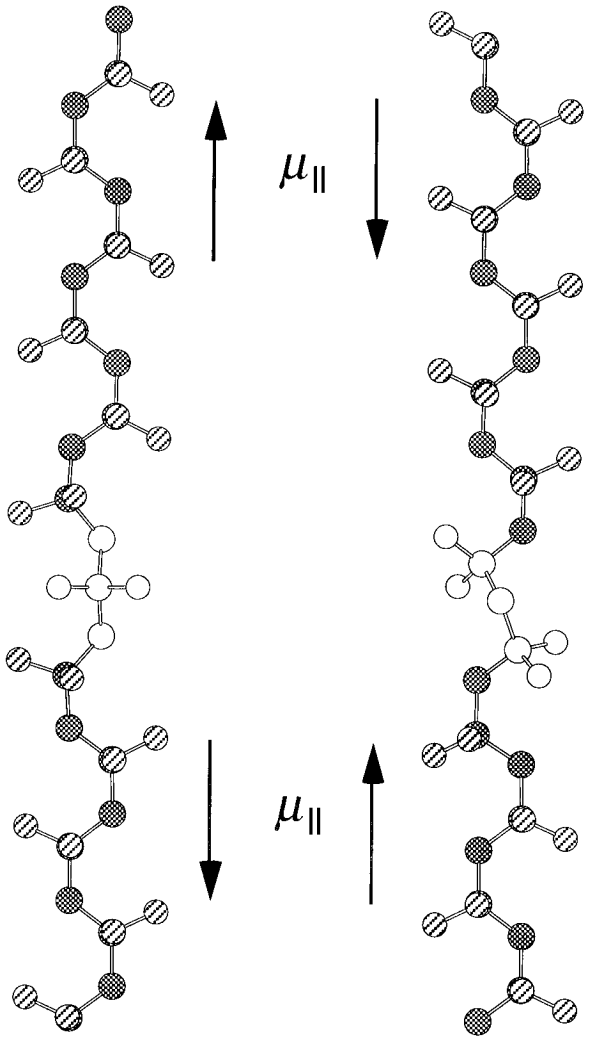

Figure 4. Divergent (left) and convergent (right) boundary conditions in α-PVDF.

3.3. Identification of Defects for the α_c Relaxation. Applying the conformational search algorithm with fixed bond lengths and bond angles and seven variable torsions results in anywhere from 0 to 100 solutions for any particular boundary condition. For a transformed segment with zero *c*-axis translation, the total numbers of solutions generated from the conformational search for each of the eight boundary conditions are given in Table 1. The number of unique solutions (i.e., those which minimized to different structures) and the range in intramolecular potential energy obtained upon removal of the constraints of fixed bond length and bond angle are also given. Histograms of the final sets of defect geometries identified by this

Table 1. Solutions from Conformational Search

boundary condition[a]	total solutions	⇒ minimize	energy range[b]
	Divergent		
1−2	10	8	6.8−15.8
2−3	28	10	7.1−14.1
3−4	10	8	7.3−15.5
4−1	28	10	6.6−15.3
	Convergent		
1−2	106	27	5.5−17.4
2−3	64	21	6.0−19.6
3−4	108	26	5.3−16.5
4−1	62	22	6.1−19.8

[a] Denotes last fixed atom of first segment and first fixed atom of second segment. Atom numbering as shown in Figure 1. [b] Intramolecular only. After localized minimization.

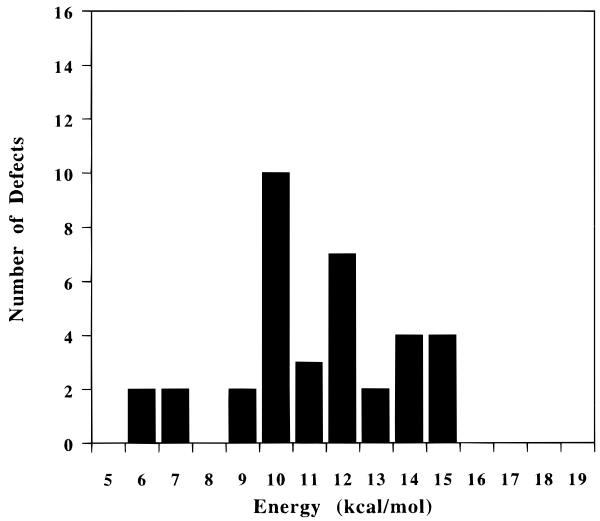

Figure 5. Histogram of defect energies for the divergent boundary conditions.

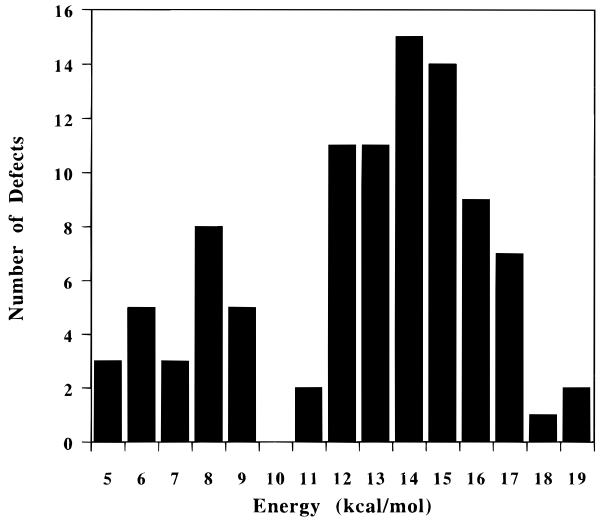

Figure 6. Histogram of defect energies for the convergent boundary conditions.

process for the divergent and convergent boundary conditions are illustrated in Figures 5 and 6.

The observed decrease in the number of unique defects indicates that there is adequate resolution in our initial discretization of conformational space. In particular, we scanned ϕ_0 in 15° increments. Rotation about a backbone torsion in a polyalkane generally results in minima separated by approximately 120°. Thus, many of the solutions we generated share the same nearest local minima. Decreasing the increment

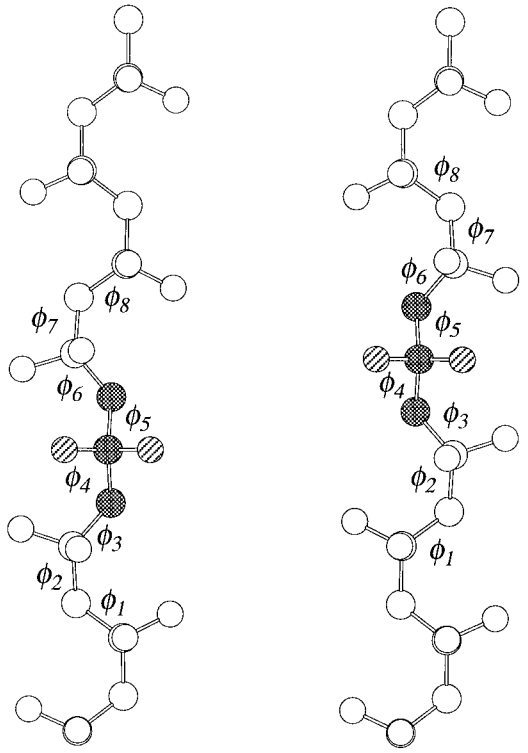

Figure 7. Candidate defects for the divergent boundary conditions: left, DIV-A; right, DIV-B.

of ϕ_0 produced many more total solutions but did not produce any new local minima. This does not imply that the conformational search is exhaustive, as the initial search is performed under the conditions of fixed bond lengths and angles.

From the reduced set of unique solutions, candidate defects were selected that had the lowest intramolecular energy and would pack into the nearest-neighbor shell with the lowest total energy. Two candidate defects were selected for both the divergent and convergent boundary conditions. The candidate defects are referred to as DIV-A and DIV-B for the divergent boundary condition (see Figure 7) and as CON-A and CON-B for the convergent boundary condition (see Figure 8). For the divergent boundary condition, there were several defects that had *intramolecular* energies lower than DIV-A and DIV-B, but all of these exhibited larger *intermolecular* energies when packed in the lattice. For the convergent boundary condition, CON-A and CON-B had both the lowest intramolecular and lowest intermolecular energies.

The backbone torsion angles of the four candidate defects are given in Table 2. When the torsion angles are numbered as in Figures 7 and 8, we observe that the torsion angles of the two defects for each transition differ only in sign. If we define a set of Cartesian coordinates with x parallel to the chain axis and z parallel to the a axis, then the two defects for each transition are related by the symmetry element $\sigma_g(xz)$—a glide plane that combines a mirror plane parallel to the xz plane and translation of $^1/_2$ the c-axis along x. This symmetry operator is also an element of the one-dimensional space group of the single chain, as shown in Figure 1.

Finally, the change in potential energy attributed to defect formation, ΔU, was determined by minimizing the four central repeat units of a six repeat unit chain containing the defect in a rigid shell of nearest-neighbor chains. Figure 3 shows the divergent defect DIV-A and

Table 2. Backbone Torsion Angles of Candidate Defects

	ϕ_1	ϕ_2	ϕ_3	ϕ_4	ϕ_5	ϕ_6	ϕ_7	ϕ_8
DIV-A[a]	174.4	79.2	−173.8	−141.2	143.5	173.7	−80.5	−174.5
DIV-B[a]	−174.6	−79.1	173.8	141.6	−143.1	−173.7	79.9	174.2
CON-A[b]	175.9	−65.6	−133.0	−65.0	−89.2	−101.0	−73.7	−178.0
CON-B[b]	−175.9	65.7	133.3	65.1	90.2	100.6	74.2	177.5

[a] Torsion angle numbers are in correspondence with Figure 7. [b] Torsion angle numbers are in correspondence with Figure 8.

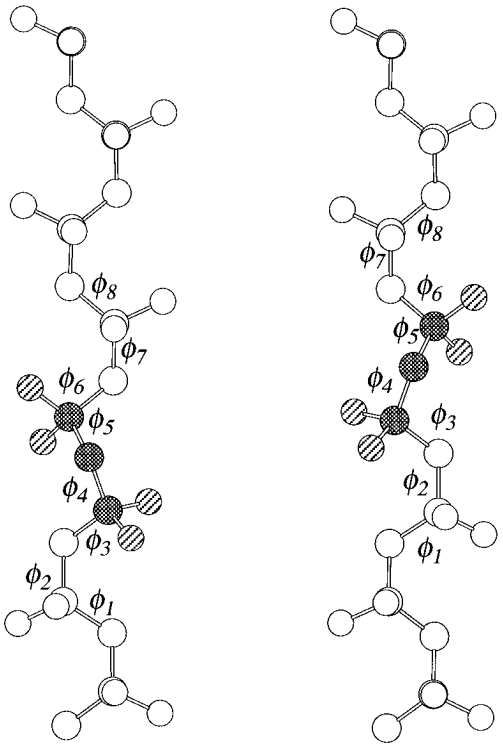

Figure 8. Candidate defects for the convergent boundary conditions: left, CON-A; right, CON-B.

Table 3. Energy of Defect Formation

	DIV-A	DIV-B	CON-A	CON-B
ΔU^{Intra}	11.1	11.1	1.2	1.3
$\Delta U^{\text{Inter}}_{\text{vdW}}$	3.2	3.2	3.0	3.2
$\Delta U^{\text{Inter}}_{\text{Coul}}$	0.2	0.2	16.0	17.0
ΔU^{total}	14.5	14.5	20.2	21.5

the shell of nearest-neighbor chains after this step. All the defects studied comprised stable local minima with positive normal-mode frequencies. Inclusion of the neighboring repeat units along the chain in this final minimization did not indicate any tendency for the defects to spread over more than a single repeat unit.

ΔU is expressed as the sum of the change in intramolecular energy, intermolecular van der Waals energy, and intermolecular Coulombic energy

$$\Delta U = \Delta U^{\text{Intra}} + \Delta U^{\text{Inter}}_{\text{vdW}} + \Delta U^{\text{Inter}}_{\text{Coul}} \qquad (6)$$

These contributions are given in Table 3. All four defects have roughly the same contribution from $\Delta U^{\text{Inter}}_{\text{vdW}}$. For the divergent boundary condition, both DIV-A and DIV-B have identical energies. ΔU for these defects arises primarily from an increase in the intramolecular energy; ΔU^{Intra} contributes 77% of the total, and $\Delta U^{\text{Inter}}_{\text{Coul}}$ contributes little more than 1%. This is in contrast to the convergent boundary condition where $\Delta U^{\text{Inter}}_{\text{Coul}}$ contributes 79% of the total while ΔU^{Intra} contributes approximately 5%. The difference of more than 1 kcal/mol in ΔU for CON-A and CON-B

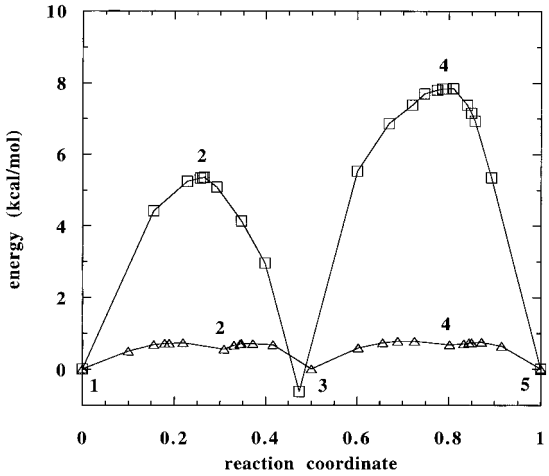

Figure 9. Periodic potential energy barriers to defect transport: (△) divergent boundary conditions; (□) convergent boundary conditions.

is due primarily to the difference in $\Delta U^{\text{Inter}}_{\text{Coul}}$. In all cases, the intermolecular mismatch energy associated with the insertion of the transformed segment into the perfect lattice is small, less than 1 kcal/mol per repeat unit. Clearly the convergent defects, CON-A and CON-B, have more significant interactions with the neighboring chains than do the divergent defects, DIV-A and DIV-B. The calculated ΔU of the divergent defects should be less sensitive to such details as the orientation of the nearest-neighbor chains, whereas the convergent defects should be much more so. Conversely, the divergent defects should be more sensitive to constitutional defects such as head-to-head and tail-to-tail junctions which alter the intramolecular energetics. Based on energetics alone, the divergent defects would appear to be more likely than the convergent defects.

3.4. Reaction Pathways for the α_c Relaxation in α-PVDF. The reaction pathways for each of the four defects, DIV-A, DIV-B, CON-A, and CON-B, which correspond to propagation of the defect by one period of the crystal lattice in the chain direction, were determined as outlined in section 2.3. The potential energies along the pathway are shown in Figure 9. The curves for CON-A and CON-B represent two distinct pathways which are nearly identical in energy; only the results for CON-A are shown. The divergent defects DIV-A and DIV-B do not have unique pathways but instead were found to be separate minima along the same pathway. The most striking difference between the reaction pathways for the divergent and convergent defects is the height of the potential energy barriers. The reaction pathway for the convergent defects has two transition states with relative potential energies of 5.7 and 8.3 kcal/mol. The reaction pathway for the divergent defects has four transition states, all with relative potential energies between 0.7 and 0.8 kcal/mol. The potential energy barriers for the transport of the divergent defects are comparable to $k_B T$ at the transition temperature of 373 K.

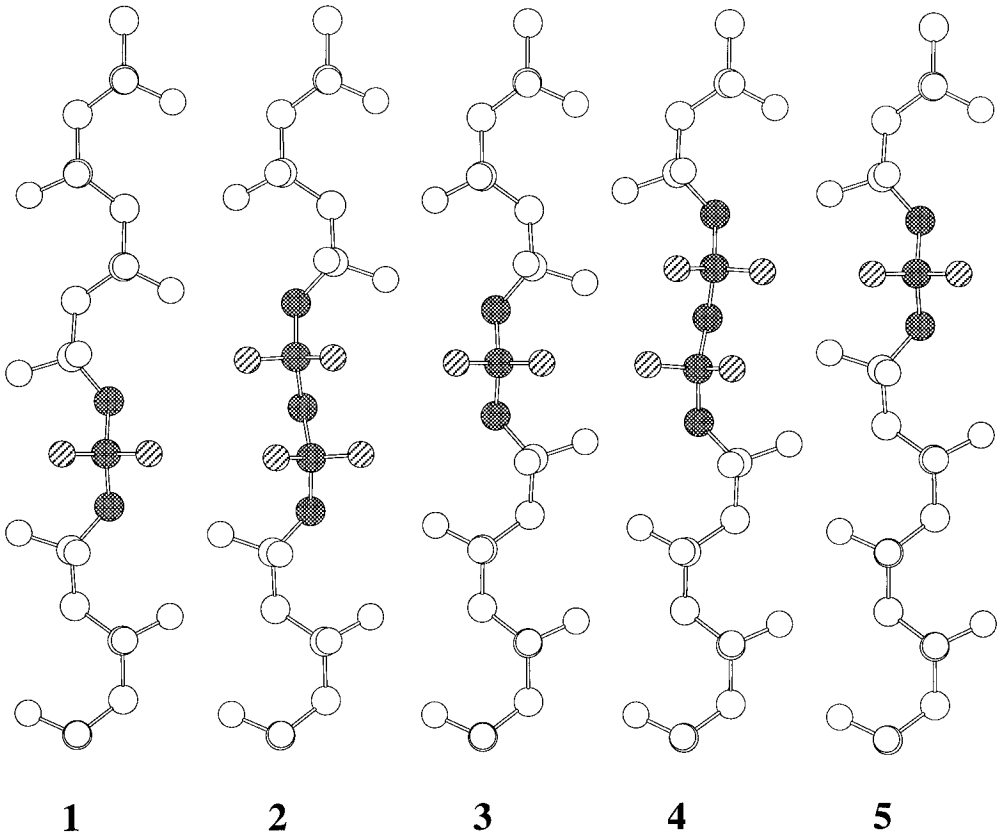

Figure 10. Defect conformations along the reaction pathway for the divergent boundary conditions. The conformations are numbered in correspondence with Figure 9.

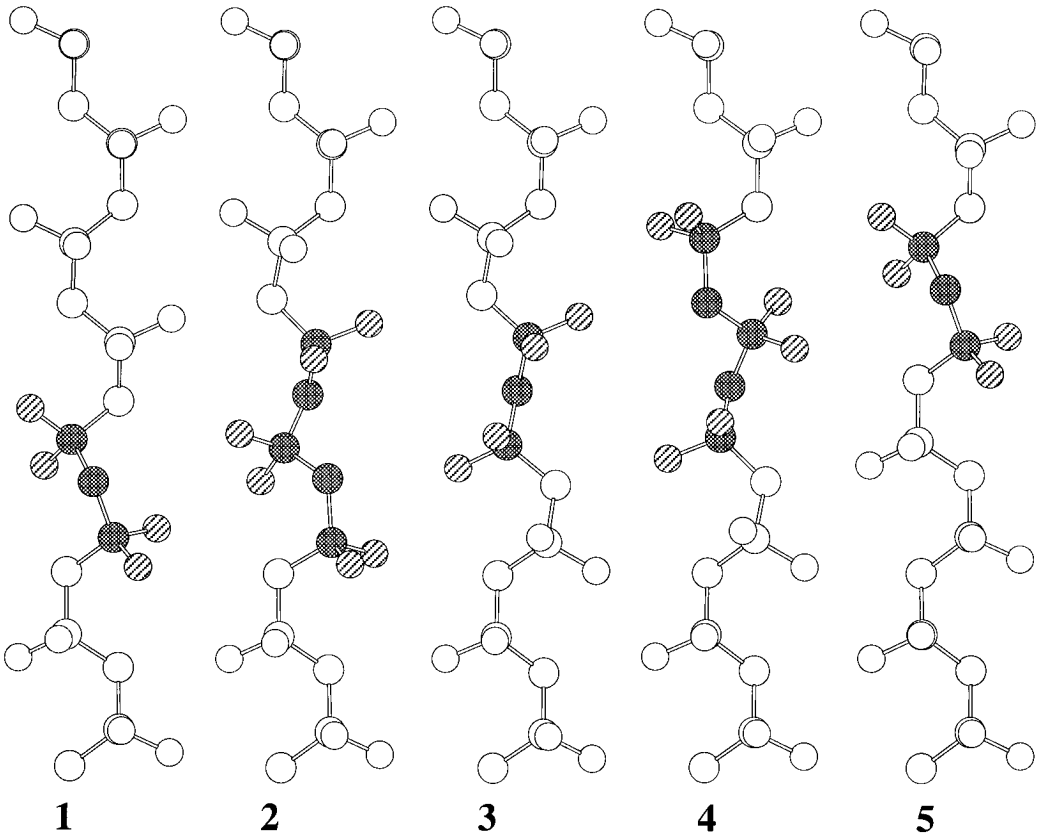

Figure 11. Defect conformations along the reaction pathway for the convergent boundary conditions. The conformations are numbered in correspondence with Figure 9.

Several conformations along the reaction pathways for the divergent and convergent defects are shown in Figures 10 and 11, respectively. For the convergent defect structures 1, 3, and 5 are minima, while 2 and 4 are transition states. Structures 1 and 5 are both CON-A separated by one repeat unit. Structure 3 is a

Table 4. Thermodynamics of Defect Formation at 373 K (kcal/mol Defect)

property	perfect chain	DIV-A	CON-A
ZPE	199.9	199.7	199.7
$E^{vib}(373) - ZPE$	29.3	29.4	29.2
$S^{vib}(373)$ (cal/mol K)	156.7	158.7	156.0
$A^{vib}(373) - A^{vib}(0)$	−29.1	−29.8	−29.0
$\Delta E^{vib}(373)$	0.0	−0.1	−0.3
$\Delta S^{vib}(373)$ (cal/mol K)	0.0	2.0	−0.7
$\Delta A^{vib}(373)$	0.0	−0.9	−0.1
ΔU	0.0	14.5	20.2
$\Delta A(373)$	0.0	13.6	20.1

minimum that was not identified during the search for defects in torsion angle space. For the divergent defects all the structures shown in Figure 10 are minima, each separated by a transition state. Structures 1 and 5 are both DIV-A separated by one repeat unit. Structure 3 is DIV-B. Structures 2 and 4 were also identified during the search of defect conformation space and found to have higher packing energies than DIV-A and DIV-B, in agreement with the reaction pathway calculations. All of the stationary points (maxima and minima) were verified by normal-mode analysis. The local minima had all positive normal-mode frequencies, and the transition states were true saddle points that had one imaginary normal-mode frequency.

3.5. Defect Thermodynamics. The probability of defect formation is proportional to $\exp(-\Delta A/k_B T)$, where ΔA is the change in free energy on defect formation. In classical kinetic theory, the rate of defect transport is proportional to $\exp(-\Delta A^*/k_B T)$, where ΔA^* is the free-energy barrier to defect transport. Here we calculate the Helmholtz free energy given by

$$A = U + A^{vib} \tag{7}$$

where U is the potential energy and A^{vib} is the vibrational Helmholtz free energy—calculated here in the harmonic approximation. The vibrational free energy can be written as

$$A^{vib} = E^{vib} - TS^{vib} \tag{8}$$

where E^{vib} and S^{vib} are the vibrational energy and entropy, respectively. The vibrational free energy of polyalkane chains is dominated by the low-frequency torsional modes. Defect formation and transport involves large changes in the torsion angles which can result in significant changes in the vibrational free energy. Changes in the low-frequency normal-modes affect the vibrational free energy in several ways. A decrease in frequency, ω, results in (i) a decrease in the zero-point energy, $ZPE = 1/2\hbar\omega$; (ii) an increase in the temperature-dependent vibrational energy, $E^{vib}(T) - ZPE$; and (iii) an increase in the vibrational entropy, $S^{vib}(T)$.

The vibrational free-energy functions of defect formation are given in Table 4. The vibrational free-energy functions of the important conformations along the reaction pathways for the divergent and convergent defects are given in Tables 5 and 6, respectively. The vibrational partition function for a transition state includes only the real normal-mode frequencies. The 1 degree of freedom corresponding to the reaction pathway at the transition state—and having an imaginary normal-mode frequency—is not included. This loss in a degree of freedom results in a negative value ΔS^{*vib} and a positive contribution to ΔA^{*vib}. The inclusion of the vibrational partition function will tend to increase the free-energy barriers for defect transport. This effect is especially significant for the divergent boundary conditions where the potential energy barriers for defect transport are less than 1 kcal/mol. The inclusion of the vibrational free energy increases the free-energy barriers by 1−2 kcal/mol.

3.6. Comparison with Experiment. The estimates of ΔA and ΔA^* determined in this work are admittedly approximate. No allowance was made for the response of the neighboring chains on the crystal lattice to the presence of the defect or for the statistical disorder of chain orientations in the crystal. We believe inclusion of such effects will tend to lower the free energies, in general, making our estimates upper bounds.

It is clear from Figures 10 and 11 that the mechanism of defect formation and subsequent propagation through the lattice is not a simple process. Nevertheless, if we interpret the experimentally observed α_c relaxation as a simple process with Arrhenius behavior, then the relaxation time of $\tau = 20$ ms estimated by NMR at 373 K corresponds to an activation free energy of $\Delta G \approx 20$ kcal/mol. An activation free energy $\Delta G \approx 16$ kcal/mol was obtained by Yano[31] using a fit of the dielectric relaxation data to the Arrhenius equation. Similarly, an activation enthalpy $\Delta H \approx 21-25$ kcal/mol was obtained by Nakagawa *et al.*[32] Miyamoto reports an activation free energy $\Delta G \ll 1$ kcal/mol obtained from a fit to a two-site model of the dielectric increment as a function of temperature. Their value is apparently given per mole of repeat units, while the others given above are per mole of activated states. (The number of repeat units in a typical lamellae of α-PVDF is 50−100.) The activation free energies calculated here, given the level of approximation, indicate that both the convergent and divergent transitions are reasonable mechanisms for the α_c relaxation.

4. Conclusions

The proposed scheme for identifying and characterizing molecular mechanisms for local relaxations occurring in crystalline polymers appears to offer an objective approach to capturing a rich variety of behavior. The conformational changes required to accommodate the

Table 5. Thermodynamics of Defect Transport at 373 K—Divergent Boundary Conditions (kcal/mol defect)[a]

property	1 (DIV-A)	1−2	2	2−3	3 (DIV-B)	3−4	4	4−5 (DIV-A)
ZPE	199.7	199.9	200.2	200.0	199.7	199.9	200.2	200.0
$E^{vib}(373) - ZPE$	29.4	28.7	29.3	28.7	29.4	28.7	29.3	28.7
$S^{vib}(373)$ (cal/mol K)	158.7	153.0	159.4	153.2	158.7	153.1	159.7	153.2
$A^{vib}(373) - A^{vib}(0)$	−29.8	−28.4	−30.1	−28.5	−29.8	−28.4	−30.2	−28.5
$\Delta E^{*vib}(373)$	0.0	−0.5	0.4	−0.4	0.0	−0.5	0.4	−0.4
$\Delta S^{*vib}(373)$ (cal/mol K)	0.0	−5.7	0.7	−5.5	0.0	−5.6	1.0	−5.5
$\Delta A^{*vib}(373)$	0.0	1.6	0.2	1.6	0.0	1.6	0.1	1.6
ΔU^*	0.0	0.7	0.6	0.7	0.0	0.8	0.7	0.7
$\Delta A^*(373)$	0.0	2.3	0.8	2.3	0.0	2.4	0.8	2.3

[a] Numbers are in correspondence with Figures 9 and 10.

Table 6. Thermodynamics of Defect Transport at 373 K—Convergent Boundary Conditions (kcal/mol defect)[a]

property	1 (CON-A)	2	3	4
ZPE	199.7	200.0	200.9	200.1
$E^{vib}(373) - ZPE$	29.2	28.6	29.2	28.6
$S^{vib}(373)$ (cal/mol K)	156.0	152.5	158.7	152.8
$A^{vib}(373) - A^{vib}(0)$	−29.0	−28.3	−30.0	−28.4
$\Delta E^{*vib}(373)$	0.0	−0.3	1.2	−0.2
$\Delta S^{*vib}(373)$ (cal/mol K)	0.0	−3.5	2.7	−3.2
$\Delta A^{*vib}(373)$	0.0	1.0	0.2	1.0
ΔU^*	0.0	5.7	−0.3	8.0
$\Delta A^*(373)$	0.0	6.7	−0.1	9.0

[a] Numbers are in correspondence with Figures 9 and 11.

α_c relaxation in α-PVDF poses a reasonable test of the utility of this procedure. For conditions mandated by experimental observation, we identified two sets of boundary conditions—referred to as divergent and convergent. For the convergent boundary conditions, two candidate defects were identified that had similar energy, structure, and barriers to defect transport. The defects with convergent boundary conditions interact significantly with the surrounding chains and have higher energies of formation and barrier heights than the defects with divergent boundary conditions. The free energy of formation of defects with divergent boundary conditions arises primarily from the change in intramolecular potential energy, and the potential energy barriers to transport are approximately equal to k_BT at the relaxation temperature of 373 K.

The formation and propagation of divergent defects introduces all-trans segments embedded in the α-PVDF conformation. The fluorines in the all-trans segment stagger to relieve steric interactions between fluorines. The propensity for formation of such a segment may offer insight into the α-to-γ transition, which involves a change in conformation from TGTḠ to $T_3GT_3\bar{G}$, and the α-to-β transition, which involves a change in conformation of TGTḠ to all-trans. The energetics of the divergent defects may be significantly affected by the presence of head-to-head and tail-to-tail junctions. These junctions are thought to stabilize the all-trans conformation relative to the TGTḠ conformation.[33]

Acknowledgment. The authors are grateful to the National Science Foundation (CTS 9457111) for financial support of this work.

References and Notes

(1) Boyd, R. H. *Polymer* **1985**, *26*, 1123 and references therein.
(2) Reneker, D. H.; Fanconi, B. M.; Mazur, J. *J. Appl. Phys.* **1977**, *48*, 4032.
(3) Reneker, D. H.; Mazur, J. *Polymer* **1982**, *23*, 401.
(4) Reneker, D. H.; Mazur, J. *Polymer* **1988**, *29*, 3.
(5) Mansfield, M.; Boyd, R. H. *J. Polym. Sci., Polym. Phys.* **1978**, *16*, 1227.
(6) Mansfield, M. *Chem. Phys. Lett.* **1980**, *69*, 383.
(7) Skinner, J. L.; Wolynes, P. G. *J. Chem. Phys.* **1980**, *73*, 4015.
(8) Skinner, J. L.; Wolynes, P. G. *J. Chem. Phys.* **1980**, *73*, 4022.
(9) Skinner, J. L.; Park, Y. H. *Macromolecules* **1984**, *17*, 1735.
(10) Schaefer, D.; Spiess, H. W.; Suter, U. W.; Fleming, W. W. *Macromolecules* **1990**, *23*, 3431.
(11) Syi, J. L.; Mansfield, M. L. *Polymer* **1988**, *29*, 987.
(12) Rutledge, G. C.; Suter, U. W. *Macromolecules* **1992**, *25*, 1546.
(13) Miyamoto, Y.; Hideki, M.; Asai, K. *J. Polym. Sci., Polym. Phys.* **1980**, *18*, 597.
(14) Takahashi, Y.; Miyaji, K. *Macromolecules* **1983**, *16*, 1789.
(15) Hirschinger, J.; Schaefer, D.; Spiess, H. W.; Lovinger, A. J. *Macromolecules* **1991**, *24*, 2428.
(16) Clark, J. D.; Taylor, P. L.; Hopfinger, A. J. *J. Appl. Phys.* **1981**, *52*, 5903.
(17) Gō, N.; Scheraga, H. A. *Macromolecules* **1970**, *3*, 178.
(18) Cottrell, A. H. *The Theory of Dislocations*; Gordon and Breach: New York, 1964.
(19) Dodd, L. R.; Boone, T. D.; Theodorou, D. N. *Mol. Phys.* **1993**, *78*, 961.
(20) Krishna Pant, P. V.; Theodorou, D. N. *Macromolecules* **1995**, *28*, 7224.
(21) Press, W. H.; Flannery, B. P.; Teukolsky, S. A.; Vetterling, W. T. *Numerical Recipes: The Art of Scientific Programming (FORTRAN version)*; Cambridge University Press: Cambridge, U.K., 1989.
(22) Flory, P. J. *Macromolecules* **1974**, *7*, 381.
(23) McCullough, R. L. *J. Macromol. Sci., Phys.* **1974**, *B9*, 97.
(24) Theodorou, D. N.; Suter, U. W. *Macromolecules* **1985**, *18*, 1467.
(25) Fischer, S.; Karplus, M. *Chem. Phys. Lett.* **1992**, *194*, 252.
(26) Cerjan, C. J.; Miller, W. H. *J. Chem. Phys.* **1981**, *75*, 2800.
(27) McQuarrie, D. A. *Statistical Mechanics*; Harper-Collins: New York, 1976.
(28) Karasawa, N.; Goddard, W. A. *Macromolecules* **1992**, *25*, 7268.
(29) Carbeck, J. D.; Lacks, D. J.; Rutledge, G. C. *J. Chem. Phys.* **1995**, *108*, 10347.
(30) Carbeck, J. D.; Rutledge, G. C. *Polymer* **1996**, in press.
(31) Yano, S. *J. Polym. Sci., Polym. Phys. Ed.* **1970**, *8*, 1057.
(32) Nakagawa, K.; Ishida, Y. *J. Polym. Sci., Polym. Phys.* **1973**, *11*, 1503.
(33) Kepler, R. G.; Anderson, R. A. *Adv. Phys.* **1992**, *41*, 1.

MA960165L